JOURNAL OF THERMOPHYSICS AND HEAT TRANSFER
Vol. 23, No. 3, July–September 2009

# Natural Convection over Vertical Plates: Local-Nonsimilarity Slip Flow Solutions

Kang Cao* and John Baker†
*University of Alabama, Tuscaloosa, Alabama 35487*

DOI: 10.2514/1.37418

**Natural convection over a vertical isothermal plate has been modeled with first-order momentum and thermal discontinuities at the wall. A local-nonsimilarity transformation has been applied and numerical solutions were obtained based on the three-equation model. The presence of nonequilibrium at the wall has been found to result in a nonsimilar boundary-layer problem. Nonsimilar velocity and temperature distributions within the boundary layer have been obtained. Results are presented which indicate the effects of nonequilibrium on wall slip velocity, temperature jump, wall shear stress, and boundary-layer thickness for both gaseous and liquid flows. Equations for predicting the drag and average Nusselt number have been formulated as an integral function of the nonequilibrium parameter. A reduction in heat transfer was predicted for more rarified gaseous flows with simultaneous momentum slip and thermal jump conditions. In liquids, without a thermal jump, heat transfer was found to increase relative to the respective no-slip value.**

## Nomenclature

| | | |
|---|---|---|
| $C_f$ | = | skin friction coefficient |
| $F$ | = | reduced stream function |
| $f$ | = | momentum accommodation coefficient |
| $G$ | = | $\xi$ derivative of $F$ |
| $Gr$ | = | Grashof number |
| $g$ | = | gravitational acceleration |
| $H$ | = | $\xi$ derivative of $G$ |
| $h$ | = | heat transfer coefficient |
| $Kn$ | = | Knudsen number |
| $k$ | = | thermal conductivity |
| $L$ | = | characteristic length |
| $Nu$ | = | Nusselt number |
| $Pr$ | = | Prandtl number |
| $p$ | = | pressure |
| $T$ | = | temperature |
| $u$ | = | streamwise velocity |
| $v$ | = | normal velocity |
| $x$ | = | coordinate along the plate |
| $y$ | = | coordinate normal to the plate |
| $\alpha$ | = | thermal accommodation coefficient |
| $\beta$ | = | volumetric thermal expansion coefficient |
| $\gamma$ | = | specific heat ratio of air |
| $\delta$ | = | boundary-layer thickness |
| $\eta$ | = | similarity variable |
| $\theta$ | = | dimensionless temperature |
| $\lambda$ | = | mean free path |
| $\mu$ | = | dynamic viscosity |
| $\nu$ | = | kinematic viscosity |
| $\xi$ | = | dimensionless nonsimilarity variable |
| $\tau$ | = | shear stress |
| $\phi$ | = | $\xi$ derivative of $\theta$ |
| $\chi$ | = | $\xi$ derivative of $\phi$ |
| $\Psi$ | = | stream function |

*Subscripts*

| | | |
|---|---|---|
| $L$ | = | length of plate |
| slip | = | slip condition |
| $w$ | = | wall boundary |
| $x$ | = | local streamwise position |
| $\infty$ | = | ambient conditions |

Received 5 March 2008; accepted for publication 6 February 2009. Copyright © 2009 by the American Institute of Aeronautics and Astronautics, Inc. All rights reserved. Copies of this paper may be made for personal or internal use, on condition that the copier pay the $10.00 per-copy fee to the Copyright Clearance Center, Inc., 222 Rosewood Drive, Danvers, MA 01923; include the code 0887-8722/09 $10.00 in correspondence with the CCC.

*Research Assistant, Department of Mechanical Engineering. Student Member AIAA.

†Associate Professor, Department of Mechanical Engineering. Senior Member AIAA.

## I. Introduction

NATURAL convection from an isothermal vertical plate is an important transport process and finds uses in many engineering applications. Over the past few decades, extensive studies have been conducted that focus on natural convection over a flat surface. Early efforts mainly sought the similarity characteristics within the boundary-layer framework. Similarity solutions were used by Ostrach [1] to analyze boundary-layer natural convective flow and heat transfer from an isothermal plate. Similarity approaches were then applied by many researchers to a wide range of engineering problems involving natural convection and were even extended to mixed convection [2,3]. Nevertheless, not all natural convection problems admit similar solutions. Sparrow et al. [4,5] treated several nonsimilar boundary-layer problems using both local-similarity and local-nonsimilarity methods. To study the flow behavior outside the boundary layer, singular perturbation methods were then employed to examine the interaction of the boundary layer with the external flow [6–9].

All of the aforementioned studies were conducted upon the basis of a continuum flow regime. Convective slip flows have recently gained interest due to the rapid development of microelectromechanical systems [10]. Natural convection processes are also of great importance to the thermal management of near-space platforms operating in very low-density and low-pressure environments [11]. As the mean free path of the flow becomes comparable to the characteristic length scale, flows will exhibit noncontinuum phenomena as a result of the deviation from interfacial thermodynamic equilibrium due to fewer collisions within the dimension of interest. The degree of the rarefaction for gaseous flows is usually characterized by the Knudsen number, defined as the ratio of molecular mean free path to the characteristic length of the problem of interest, given as [12]

$$Kn = \lambda / L \tag{1}$$

According to the value of Knudsen number, the flows can be classified into three categories: continuum flow ($Kn < 0.01$), slip flow ($0.01 \leq Kn \leq 0.1$), and transitional flow ($0.1 < Kn < 10$) [13].

As the flow approaches the continuum limit, the conventional no-slip wall boundary conditions fail to accurately model the surface interaction between the fluid and the wall boundary due to the low molecular collision frequency [13]. Slip models have been proposed to ameliorate the prediction of the nonequilibrium phenomenon near wall boundaries within the framework of the continuum assumption. For gaseous flows, the Maxwell slip model relates the slip velocity at the wall to the local velocity gradient based on the gas kinetic theory, given by [14]

$$u_{\text{slip}} \approx \left(\frac{2}{f}-1\right)\lambda \left.\frac{\partial u}{\partial y}\right|_w \tag{2}$$

The original Maxwell model has been extended to a high-order form by including an empirical slip coefficient $C_s$ as a function of the Knudsen number [15]:

$$u_{\text{slip}} = \left(\frac{2}{f}-1\right)C_s(Kn)L \left.\frac{\partial u}{\partial y}\right|_w \tag{3}$$

Note that the original Maxwell slip condition is recovered at the slip coefficient equal to $Kn$, which is of the first-order $Kn$ dependence. The dependence of the slip coefficient on higher-order $Kn$ has been studied by many researchers. Recent works involving the determination of empirical slip coefficients and slip models can be can be found in Bahukudumbi et al. [16], Beskok [17], Pan et al [18], and Bayazitoglu and Tunc [19]. The performance of several proposed empirical slip models was investigated by McNenly et al. [20] by comparing the simulation results with the Direct Simulation Monte Carlo data. It has been found that all tested slip models are fairly accurate for near equilibrium conditions at $Kn < 0.1$, but the error will increase with an increasing Knudsen number.

For liquid slip flows, the linear Navier boundary condition provides an empirical model relating the slip velocity at the wall to the local shear rate by [21]

$$u_{\text{slip}} \approx l_s \left.\frac{\partial u}{\partial y}\right|_w \tag{4}$$

where $l_s$ is the slip length. It has been found that the slip length depends on the liquid, geometry, and shear rate [21]. An experimental study by Tretheway and Meinhart [22] has found that the slip length for water flowing over a hydrophobic surface is approximately 1 $\mu$m.

In addition to velocity slip, as the Knudsen number grows beyond the continuum limit, a temperature jump may also exist between the gas and the wall boundary. The interfacial temperature discontinuity physically accounts for gas molecules not thermally accommodated with the wall and thus is very important to the prediction of energy transfer. Analogous to velocity slip, the kinetic theory expression for a first-order temperature jump condition is given by [21]

$$T_{\text{slip}} - T_w \approx \left(\frac{2}{\alpha}-1\right)\frac{2\gamma}{\gamma+1}\frac{\lambda}{Pr}\left.\frac{\partial T}{\partial y}\right|_w \tag{5}$$

A review of the vast body of information on slip models is beyond the scope of this effort. For a more thorough treatment of slip models for fluid flows, the reader is referred to the book by Karniadakis et al. [12].

The study of gaseous and liquid flows in microdevices, such as microchannels, have been widely conducted during the past two decades. A brief summary of previous studies can be found in literature [23–28]. Nonetheless, the literature on external convective flow with slip boundary conditions is found to be very limited. Oosthuizen [29] roughly estimated the effects of very small amounts of slip (with $Kn$ varying from $10^{-5}$ to $10^{-4}$) on the free convection from a vertical plate using the von Kármán integral approach. A slight increase was predicted in the average Nusselt number with the increasing slip condition. Eldighidy and Fathalah [30] examined the effect of momentum slip on the natural convection from a vertical plate. Temperature jump, however, was not considered in the boundary condition. It is also unclear as to which slip boundary conditions were developed. The transformed governing equations, however, indicate the solutions were based on local-similarity methods. The results showed that velocity and heat transfer at the plate will be enhanced with the increasing $Kn$. Martin and Boyd [31] investigated forced convection over a horizontal plate with slip conditions. Numerical solutions were obtained using finite difference methods. Results suggested that the flow structure, velocity profile, and boundary-layer thickness will be altered by the rarified condition. The results obtained for natural convective slip flow from an isothermal vertical plate in previous investigations are inconclusive. No study has simultaneously taken the interfacial momentum and temperature slip into account for natural convection, though the simultaneous discontinuity is vital in predicting heat transfer at microscale or in a slightly rarefied environment. In addition, few functional correlations have been obtained quantitatively relating heat transfer to the slip conditions. Therefore, our understanding of the behavior of the flow structure and heat transfer for natural convection in a slightly rarefied environment is far from complete.

The aim of this study is to provide a better understanding as to the effect interfacial velocity and temperature jump have on natural convection heat transfer. Local nonsimilar solutions to the boundary-layer equations for natural convection over a vertical isothermal plate in a slightly rarefied environment are presented in this paper. The boundary conditions and equations presented here are substantially different compared to earlier results reported in [30]. Simultaneous velocity slip and temperature jump boundary conditions were considered for gaseous slip flow, although the temperature jump is neglected for liquid flows. The change in velocity and temperature distributions, wall shear stress, and boundary-layer thickness due to the interfacial slip are analyzed in both flows. A correlation for skin friction coefficient and average heat transfer, that is, Nusselt number over the plate has been formulated in an integral form as a function of the nonequilibrium parameter and the thermophysical properties of the flow.

## II. Laminar Natural Convection with Interfacial Slip

Consider a vertical flat plate immersed in quiescent ambient fluid of temperature $T_\infty$, as shown in Fig. 1. The plate is maintained at a constant surface temperature $T_w$ ($T_w > T_\infty$). The $x$ ordinate is measured along the vertical plate from the leading edge, and the $y$ ordinate is measured normal to the plate.

The governing equations for two-dimensional, steady-state, incompressible, laminar natural convection are the continuity, momentum, and energy equations. With the boundary-layer assumption and Boussinesq approximation, these governing equations are, respectively, given as

$$\frac{\partial u}{\partial x}+\frac{\partial v}{\partial y}=0 \tag{6}$$

$$u\frac{\partial u}{\partial x}+v\frac{\partial u}{\partial y}=g\beta(T-T_\infty)+\upsilon\frac{\partial^2 u}{\partial y^2} \tag{7}$$

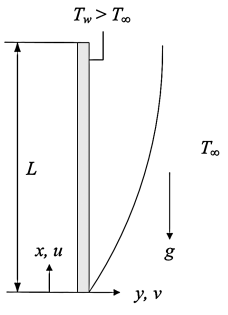


**Fig. 1 Natural convection over a vertical plate.**

$$u\frac{\partial T}{\partial x}+\upsilon\frac{\partial T}{\partial y}=\alpha\frac{\partial^2 T}{\partial y^2} \tag{8}$$

A group of dimensionless parameters are introduced to seek the local-nonsimilar solutions, including a pseudosimilarity position $\eta$, reduced stream function $F$, and dimensionless temperature $\theta$, respectively, given by

$$\eta\equiv\frac{y}{x}\left(\frac{Gr_x}{4}\right)^{1/4} \tag{9}$$

$$\psi(x,y)\equiv F(\xi,\eta)\left[4\nu\left(\frac{Gr_x}{4}\right)^{1/4}\right] \tag{10}$$

$$\theta\equiv(T-T_\infty)/(T_s-T_\infty) \tag{11}$$

### A. Interfacial Slip Boundary Conditions

First consider the wall boundary conditions for gaseous flows in the slip regime. The starting point for the slip condition is Maxwell's first-order slip model. Two interfacial discontinuities involving momentum and energy transfer, given by Eqs. (2) and (5), are used to replace the no-slip conditions for nonrarefied flows. In light of the defined dimensionless variables, the velocity slip and temperature jump boundary conditions can be transformed into the following forms:

$$F'(0)=\left(\frac{2}{f}-1\right)Kn_x\left(\frac{Gr_x}{4}\right)^{1/4}F''(0) \tag{12}$$

$$\theta(0)=\frac{1}{Pr}\left(\frac{2}{\alpha}-1\right)Kn_x\left(\frac{Gr_x}{4}\right)^{1/4}\frac{2\gamma}{\gamma+1}\left.\frac{\partial\theta}{\partial\eta}\right|_w+1 \tag{13}$$

where prime denotes the derivative with respective to $\eta$, $Kn_x$ is the local Knudsen number defined as $\lambda/x$, $Gr_x$ is the local Grashof number, and $\gamma$ is $\frac{7}{5}$ for a diatomic gas, $\frac{5}{3}$ for a monatomic gas, and approximately 1.0 for a liquid [21]. Experiments have shown that the momentum and thermal accommodation coefficients are fairly close to unity for rough surfaces where molecules are reflected by the wall at random angles uncorrelated with their entry angle [14]. To develop a tractable analysis, the present paper considers the fully diffuse situation only, where $f$ and $\alpha$ are both assumed to be unity. In practice, the slip model can also be easily adapted for any actual accommodation coefficients obtained from experiments.

Note that the preceding slip conditions are dependent upon the streamwise location $x$. In this regard, the nonsimilarity variable $\xi$ is defined to describe the surface location dependence of $x$:

$$\xi=Kn_x\left(\frac{Gr_x}{4}\right)^{1/4} \tag{14}$$

Similarly, in liquid flows, the Navier slip boundary conditions based on Eq. (4) can be transformed to

$$F'(0)=\left(\frac{2}{f}-1\right)\frac{l_s}{x}\left(\frac{Gr_x}{4}\right)^{1/4}F''(0) \tag{15}$$

Accordingly, the slip parameter for liquid flow has the form

$$\xi=\frac{l_s}{x}\left(\frac{Gr_x}{4}\right)^{1/4} \tag{16}$$

where $l_s/x$ may be viewed as the dimensionless local slip length for liquid flow.

Despite the different definitions of $\xi$ in gaseous and liquid flows, the nonsimilarity parameter bears similar physical meanings in both flows. First, note the value of $\xi$ varies in a sense opposite to $x^{-1/4}$, and hence it can be used to describe the streamwise location along the plate. Second, $\xi$ controls the slip boundary conditions. The magnitude of $\xi$ can be used to quantitatively characterize the degree of nonequilibrium at the wall or, in other words, how much the flow deviates from the no-slip condition. For instance, if $\xi$ approaches zero, indicating $x$ location is far away from the leading edge of the plate, the slip effect will be negligible and thus the no-slip boundary condition applies. On the other hand, a larger value of $\xi$ indicates that the boundary condition will deviate more from the no-slip condition. As $\xi$ approaches infinity, the velocity slip and temperature jump will become infinitely large, giving a nearly uniform velocity and temperature distribution with the ambient condition:

$$F'=0,\qquad \theta=0\quad \text{as } \xi\to\infty \tag{17}$$

However, a more detailed speculation should be given to $\xi$ of large values. A large value $\xi$ corresponds to a small $x$, in other words, the leading edge of the plate. However, at the leading edge, the boundary-layer assumption then is not appropriate, and, as a consequence, the boundary-layer equations become inaccurate. Moreover, if a large $\xi$ is due to a Knudsen number greater than 0.1, that is, the flow exits in the transitional or free molecular flow regime, then the Navier–Stokes equations themselves fail to accurately model the thermal and momentum transport behavior. For this reason, a discussion regarding large value $\xi$ could be prone to error in nature. Therefore, we limit the discussion in this paper for a relatively small range of $\xi$ from 0 to 5.0, as this will cover most of the slip flow region.

In addition to the two slip boundary conditions, the other boundary conditions include that for an impermeable wall, the velocity $u$ at the wall, and the dimensionless temperature $\theta$ far away from the plate, respectively, given by

$$v_w=0,\qquad u_\infty=0,\qquad \theta_\infty=0 \tag{18}$$

The latter two conditions can be easily written as

$$F'=0,\qquad \theta=0\quad \text{as } \eta\to\infty \tag{19}$$

The mathematical expression for normal velocity at the plate, however, needs more consideration, as will be seen in the following subsection.

### B. Formulation of Boundary-Layer Equations

With the boundary conditions being dependent upon the streamwise location along the plate, it suggests that the solution to the problem, that is, reduced stream function $F$ and temperature distribution $\theta$, also be a function of the streamwise location $\xi$, in addition to the variable $\eta$ in classical similarity solutions. Accordingly, the derivative relationships are modified as

$$\frac{\partial}{\partial y}=\frac{\partial}{\partial\eta}\frac{\partial\eta}{\partial y}=\frac{1}{x}\left(\frac{Gr_x}{4}\right)^{1/4}\frac{\partial}{\partial\eta} \tag{20a}$$

$$\frac{\partial^2}{\partial y^2}=\frac{\partial}{\partial\eta}\left(\frac{\partial}{\partial y}\right)\frac{\partial\eta}{\partial y}=\frac{1}{x^2}\left(\frac{Gr_x}{4}\right)^{1/2}\frac{\partial^2}{\partial\eta^2} \tag{20b}$$

$$\frac{\partial}{\partial x}=\frac{\partial}{\partial\xi}\frac{\partial\xi}{\partial x}+\frac{\partial}{\partial\eta}\frac{\partial\eta}{\partial x}=-\frac{1}{4x}\left(\xi\frac{\partial}{\partial\xi}+\eta\frac{\partial}{\partial\eta}\right) \tag{20c}$$

Therefore, the longitudinal and normal velocity components can be, respectively, expressed as

$$u=\frac{\partial\psi}{\partial y}=\frac{2\upsilon}{x}Gr_x^{1/2}F'(\xi,\eta) \tag{21}$$

$$\begin{aligned}v=-\frac{\partial\psi}{\partial x}=-\frac{\partial}{\partial x}\left[F(\xi,\eta)4\nu\left(\frac{Gr_x}{4}\right)^{1/4}\right]=-\left\{4\nu\left(\frac{Gr_x}{4}\right)^{1/4}\frac{\partial F}{\partial x}\right.\\ \left.+F\frac{\partial}{\partial x}\left[4\nu\left(\frac{Gr_x}{4}\right)^{1/4}\right]\right\}=\frac{\upsilon}{x}\left(\frac{Gr_x}{4}\right)^{1/4}\left(\eta\frac{\partial F}{\partial\eta}+\xi\frac{\partial F}{\partial\xi}-3F\right)\end{aligned} \tag{22}$$

The dimensionless longitudinal and normal velocity components may be defined as

$$u^* = \frac{u}{(2\upsilon/x)Gr_x^{1/2}} = F'(\xi,\eta) \tag{23}$$

$$v^* = \frac{v}{(\upsilon/x)(Gr_x/4)^{1/4}} = \eta\frac{\partial F}{\partial \eta} + \xi\frac{\partial F}{\partial \xi} - 3F \tag{24}$$

In terms of the preceding relations, the governing equations can be transformed to read

$$F''' + 3FF'' - 2(F')^2 + \theta = \xi\left(F''\frac{\partial F}{\partial \xi} - F'\frac{\partial F'}{\partial \xi}\right) \tag{25}$$

$$\frac{1}{Pr}\theta'' + 3F\theta' = \xi\left(\theta'\frac{\partial F}{\partial \xi} - F'\frac{\partial \theta}{\partial \xi}\right) \tag{26}$$

With the normal velocity $v$ expressed in Eq. (22), the boundary condition of $v_w = 0$ is given by

$$3F = \xi\frac{\partial F}{\partial \xi}, \quad \text{as } \eta = 0 \tag{27}$$

The other boundary conditions are stated in Eqs. (12), (13), (17), and (19).

### C. Local-Similarity Model

Before proceeding into the local-nonsimilarity method, it is useful to examine the boundary-layer Eqs. (25) and (26) from the perspective of the local-similarity concept. To derive the equations for the local-similarity model, one assumes that the terms on the right side of Eqs. (25–27) are sufficiently small so that they may be negligible. Then the local-similarity transformation gives

$$F''' + 3FF'' - 2(F')^2 + \theta = 0 \tag{28}$$

$$\frac{1}{Pr}\theta'' + 3F\theta' = 0 \tag{29}$$

The boundary conditions are summarized by

$$\begin{cases} F(0) = 0 \\ F'(0) = \xi F''(0) \\ \theta(0) = \frac{1}{Pr}\xi\frac{2\gamma}{\gamma+1}\theta'(0) + 1 \\ F'(\xi,\infty) = 0, \qquad \theta(\xi,\infty) = 0 \end{cases} \tag{30}$$

The parameter $\xi$ contained in the boundary conditions can be regarded as an assigned constant at any streamwise location along the plate. The transformed governing equations by local-similarity method are a system of ordinary differential equations, with the nonsimilar effect retained in boundary conditions. For a given value of $\xi$, the solution is independent of any other at any other $\xi$ value. Therefore, by assigning a succession of $\xi$ values along the plate, the velocity and temperature distributions can be determined.

One weakness of the local-similarity method is the accuracy. During the local-similarity transformation, the nonsimilar terms on the right side of Eqs. (25) and (26) as parts of the momentum and energy equations were lost. The local-similarity postulation requires $\xi$ be close to zero. Otherwise, the terms in parentheses on the right-hand side of the equations must be very small to justify the omission of nonsimilar terms. The validity of the latter assumption, however, is subject to uncertainty that may induce numerical inaccuracy.

### D. Local Nonsimilarity Models

The local-nonsimilar boundary-layer equations will now be derived. Unlike those nonsimilar boundary-layer problems investigated in literature [4,5], the nonsimilarity aspect for the present problem arises from the effect of interfacial momentum and thermal discontinuities at the wall. To begin with, the two-equation model will first be derived. Let

$$G(\xi,\eta) = \partial F(\xi,\eta)/\partial\xi, \qquad \varphi(\xi,\eta) = \partial\theta(\xi,\eta)/\partial\xi \tag{31}$$

Then Eqs. (25) and (26) are differentiated with respect to $\xi$, giving a set of auxiliary equations

$$G''' + 3FG'' - 3F'G' + 2F''G + \varphi = \xi\frac{\partial}{\partial\xi}[F''G - F'G'] \tag{32}$$

$$\frac{1}{Pr}\varphi'' + 3F\varphi' + F'\varphi + 2G\theta' = \xi\frac{\partial}{\partial\xi}(\theta'G - F'\varphi) \tag{33}$$

Similarly, differentiate the boundary conditions in Eqs. (12), (13), (19), and (27) to obtain additional boundary conditions

$$\begin{cases} 2G(0) = \xi\frac{\partial}{\partial\xi}G(0) \\ G'(0) = F''(0) + \xi G''(0) \\ \varphi(0) = \frac{1}{Pr}\frac{2\gamma}{\gamma+1}[\theta'(0) + \xi\varphi'(0)] \\ G'(\xi,\infty) = 0, \qquad \varphi(\xi,\infty) = 0 \end{cases} \tag{34}$$

If the right side terms containing $\xi\partial/\partial\xi$ in Eqs. (32) and (33) are neglected, then they become the subsidiary momentum and energy equations for Eqs. (25) and (26). In a like manner, the boundary conditions in Eq. (34) are auxiliary to the original ones. This is referred to as the two-equation model because the momentum and energy distribution each involves the solution to two simultaneous equations.

The preceding outlined procedures represent the first stage of the local-nonsimilarity model. Next, the governing equations for the three-equation model are briefly formulated. First, let

$$H(\xi,\eta) = \partial G/\partial\xi, \qquad \chi(\xi,\eta) = \partial\varphi/\partial\xi \tag{35}$$

Then, Eqs. (32–34) are differentiated with respect to $\xi$ and the terms containing $\xi\partial^2/\partial\xi^2$ are neglected. This transformation yields a second set of auxiliary equations and boundary conditions:

$$H''' + 3FH'' - 2F'H' + F''H + 4GG'' - 2(G')^2 + \chi = 0 \tag{36}$$

$$\frac{1}{Pr}\chi'' + 3F\chi' + 2F'\chi + 4G\varphi' + 2G'\varphi + H\theta' = 0 \tag{37}$$

$$\begin{cases} H(0) = 0 \\ H'(0) = 2G''(0) + \xi H''(0) \\ \chi(0) = \frac{1}{Pr}\frac{2\gamma}{\gamma+1}[2\varphi'(0) + \xi\chi'(0)] \\ H'(\xi,\infty) = 0, \qquad \chi(\xi,\infty) = 0 \end{cases} \tag{38}$$

In summary, all the momentum and energy equations for the three-equation model are brought together as

$$F''' + 3FF'' - 2(F')^2 + \theta = \xi(F''G - F'G') \tag{39a}$$

$$\frac{1}{Pr}\theta'' + 3F\theta' = \xi(\theta'G - F'\varphi) \tag{39b}$$

$$G''' + 3FG'' - 3F'G' + 2F''G + \varphi = \xi[GG'' + F''H - (G')^2 - F'H'] \tag{39c}$$

$$\frac{1}{Pr}\varphi'' + 3F\varphi' + F'\varphi + 2G\theta' = \xi(G\varphi' + H\theta' - G'\varphi - F'\chi) \tag{39d}$$

$$H''' + 3FH'' - 2F'H' + F''H + 4GG'' - 2(G')^2 + \chi = 0 \tag{39e}$$

$$\frac{1}{Pr}\chi'' + 3F\chi' + 2F'\chi + 4G\varphi' + 2G'\varphi + H\theta' = 0 \tag{39f}$$

with boundary conditions for $F$, $G$, $H$, $\theta$, $\phi$, and $\chi$ for the three-equation model summarized by

$$\text{as } \eta = 0 \begin{cases} 3F = \xi G, \quad 2G = \xi H, \quad H = 0 \\ F' = \xi F'', \quad G' = F'' + \xi G'' \\ H' = 2G'' + \xi H'' \\ \theta = \frac{1}{Pr}\xi\frac{2\gamma}{\gamma+1}\theta' + 1 \\ \varphi = \frac{1}{Pr}\frac{2\gamma}{\gamma+1}(\theta' + \xi\varphi') \\ \chi = \frac{1}{Pr}\frac{2\gamma}{\gamma+1}(2\varphi' + \xi\chi') \end{cases} \tag{40a}$$

$$\text{as } \eta \to \infty \begin{cases} F' = 0, \quad \theta = 0 \\ G' = 0, \quad \varphi = 0 \\ H' = 0, \quad \chi = 0 \end{cases} \tag{40b}$$

The advantage of local-nonsimilarity method is that it preserves the nonsimilar terms in original governing equations and boundary conditions with only part of the subsidiary nonsimilar terms dropped from its subsidiary equations. Because the original governing equations remain intact, the local-nonsimilarity method is expected to be more accurate than the local-similarity solution. In addition, because the nonsimilar terms are only dropped at the level of the secondarily subsidiary momentum and energy equations, the results from the three-equation model should have higher accuracy than those from the two-equation model. The reader may also wish to consult the literature [4,5] for more discussion about the numerical accuracy of the local-nonsimilarity method.

## III. Results and Discussion

The system of ordinary differential Eqs. (39a–39f) subject to boundary conditions (40a) and (40b) represent a two-point boundary value problem and needs to be solved simultaneously. They were solved numerically using the three-stage Lobatto IIIA collocation method, which provides continuous solutions of fourth-order accuracy uniformly in the problem domain. The numerical algorithm, application procedures, and validation of accuracy have been outlined in great detail in [32,33], and so will not be repeated here. Numerical solutions were first obtained for gaseous flow with simultaneous velocity and temperature slip at the wall and then for liquid flow with only the velocity slip condition. Results from the three-equation nonsimilarity model are presented for velocity and temperature distributions, wall slip velocity, wall shear stress, skin friction coefficient, and average Nusselt number over the plate.

### A. Effect of Slip and Thermal Jump in Gaseous Flow

The dimensionless $x$-velocity $F'$ as a function of position and nonequilibrium condition for $Pr$ of 0.72 is shown in Fig. 2. As previously mentioned, due to the introduction of slip at the wall, the boundary-layer velocity profile will no longer admit itself to a self-similar shape. The velocity profile in the vicinity of plate will be greatly altered by the effect of nonequilibrium. The peak velocity is seen to decrease with the increasingly rarefied condition, causing an approximately 25% decrease than the no-slip value as $\xi$ approaches 5.0. Note also the position $\eta$, at which the peak velocity is attained, will shift toward the plate. It is also seen that the velocity distribution at $\xi$ equal to zero, where slip effect is not present, becomes identical to that in the classical no-slip solution.

Figure 3 shows the temperature profile $\theta$ as a function of position and nonequilibrium for $Pr$ of 0.72. The amount of thermal jump at the wall will increase monotonically as the flow becomes more rarefied, causing more than a 75% decrease in the value of the dimensionless temperature for $\xi$ at 5.0. The amount of temperature drop of the gas near the wall is more drastic at the initial stage of rarefaction, for instance, it causes approximately 45% decrease as $\xi$ varies from the no-slip condition to 1.0. The result indicates that a small thermal jump condition at the wall boundary can have a remarkable impact on the temperature distribution within the boundary layer. This behavior of temperature distribution due to the thermal jump at the wall boundary, however, was not quantitatively revealed in any previous investigation. Again, as $\xi$ approaches zero, no temperature jump exists at the wall and the no-slip solution [34] is recovered.

Figure 4 shows the three-dimensional plot of dimensionless shear stress $F''$. As expected, a peak dimensionless shear stress of 0.6759 occurs for the no-slip conditions. The magnitude of stress decreases with the increasing rarefaction. Note that the shear stress near the plate is of positive value, representing the buoyancy driving forces for flows. As $\eta$ moves away from plate, stress gradually decreases and eventually becomes a negative value, indicating the flow is being retarded by the ambient fluid outside the boundary layer.

The wall slip velocity $F'(0)$ is shown in Fig. 5. Initially, the slip velocity increases rapidly as the flow becomes more rarefied. $F'(0)$

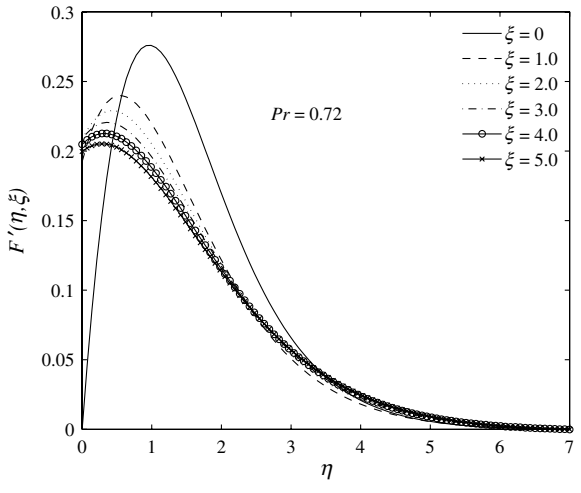


**Fig. 2 Dimensionless $x$-velocity profile.**

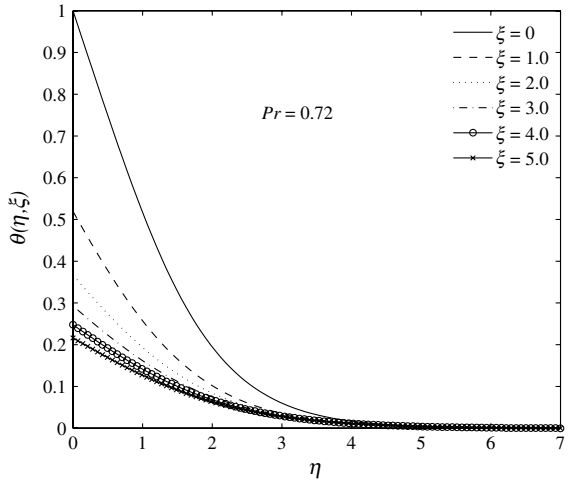


**Fig. 3 Dimensionless temperature profile.**

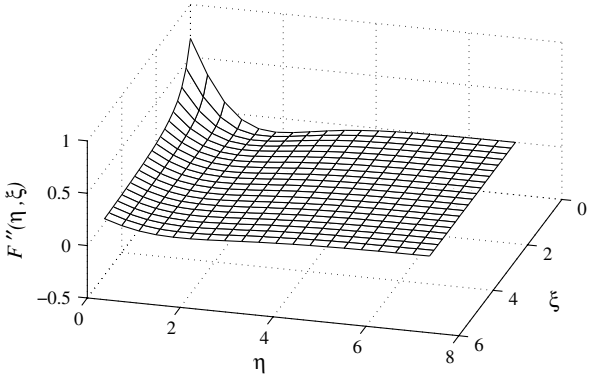


**Fig. 4 Shear stress as a function of $\eta$ and $\xi$.**

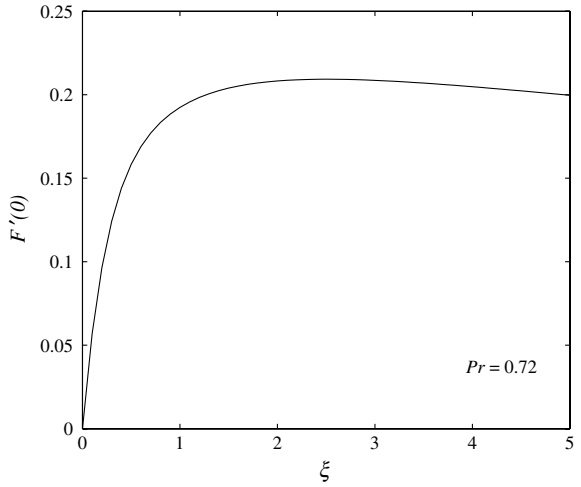


**Fig. 5 Slip velocity as a function of nonequilibrium.**

reaches the peak value of 0.2093 at $\xi$ equal to 2.5. It is also interesting to note that, rather than always increasing monotonically with the increased rarefaction, the wall slip velocity tends to decrease slowly after reaching the peak value, giving about a 5% drop from the peak value to $\xi$ at 5.0. This behavior can be justified by a closer examination of the fourth equation in Eq. (40a), which indicates the wall slip velocity will attain its peak value when the product of nonequilibrium $\xi$ and the dimensionless skin friction $F''(0)$ is maximized, as is seen shortly.

The skin friction coefficient is another physical quantity of interest. The wall shear stress can be expressed as

$$\tau_w = \mu \left.\frac{\partial u}{\partial y}\right|_{y=0} = \frac{4\mu\nu}{x^2}\left(\frac{Gr_x}{4}\right)^{3/4} F''(0) \tag{41}$$

Hence, the local friction coefficient has the form

$$C_{f,x} = \frac{\tau_{w,x}}{\rho u_0^2/2} = 2\left(\frac{Gr_x}{4}\right)^{-1/4}\frac{x}{L}F''(0) \tag{42}$$

Here, the $u_0$ is the reference velocity defined as

$$u_0 = \sqrt{g\beta(T_w - T_\infty)L}$$

The dimensionless skin friction $F''(0)$ is shown in Fig. 6. The result shows again that $F''(0)$ has a maximum value of 0.6759 at the no-slip condition. It is known from [35] that the value of $F''(0)$ in the classical no-slip condition gives 0.6760. This verifies that the result obtained by the three-equation nonsimilarity model is able to accurately converge to the classical solution at the no-slip case. In addition, the wall shear stress decreases rapidly with the increasing degree of rarefaction, that is, $F''(0)$ decreases by approximately 70% as $\xi$ varies from 0 to 1.0. Because the local skin friction is proportional to $F''(0)$, likewise it is expected to decrease monotonically as the flow becomes more rarefied. Note also that, at this point, the behavior of wall slip velocity can be examined closely. As noticed earlier, the peak slip velocity $F'(0)$ will occur when the product of $\xi$ and $F''(0)$ is maximized. In Fig. 6, $\xi F''(0)$ represents the rectangle area encompassed by respective coordinate for an arbitrary point on the curve. Therefore, peak wall slip velocity is obtained at the maximization of this area.

The total viscous drag force per unit width can be computed by integrating the wall shear stress over the entire plate of length $L$:

$$F_D = \int_0^L \tau_w \,\mathrm{d}x = 4\rho\nu^{1/2}[g\beta(T_w - T_\infty)/4]^{3/4}\int_0^L x^{1/4}F''(0)\,\mathrm{d}x \tag{43}$$

The drag coefficient is defined as [34]

$$C_D = \frac{F_D}{\frac{1}{2}\rho u_0^2 L} \tag{44}$$

Substitute the definition of nonequilibrium parameter $\xi$ in to Eq. (43) and change the integration with respect to $\xi$, then the expression for drag coefficient is derived as an integral formula

$$\frac{C_D}{(Gr_L/4)^{-1/4}} = 8\xi_L^5\int_{\xi_L}^{\infty}\xi^{-6}F''(0)\,\mathrm{d}\xi \tag{45}$$

where $\xi_L$ is the nonsimilarity variable $\xi$ evaluated at length $L$. Note that, with a given Prandtl number, $F''(0)$ is a function of the nonsimilarity variable $\xi$. The functional relation between $F''(0)$ and $\xi$ may be obtained by fitting to the curve shown in Fig. 6 to get

$$F''(0) = \frac{3.614}{5.349 + 13.39\xi^{1.138}}, \qquad (Pr = 0.72) \tag{46}$$

The coefficient of determination of Eq. (46) is 0.999985. Then, the drag coefficient $C_D/(Gr_L/4)^{-1/4}$ was obtained by substituting Eq. (46) into Eq. (45) for numerical integration. The drag coefficient as a function of nonequilibrium for $Pr$ of 0.72 is plotted in Fig. 7.

The result shows that the drag coefficient decreases rapidly with the increasing nonequilibrium condition, giving an approximately 95% drop as $\xi_L$ varies from 0 to 5.0. At $\xi_L$ equal to zero, $C_D/(Gr_L/4)^{-1/4}$ gives approximately 1.0804, and this value can be checked by the classical no-slip solution. At the no-slip condition, $F''(0)$ is independent of $\xi$, for it is a function of the Prandtl number only. Therefore, $F''(0)$ in Eq. (45) can be moved outside of the integral and the drag coefficient for the no-slip case given by

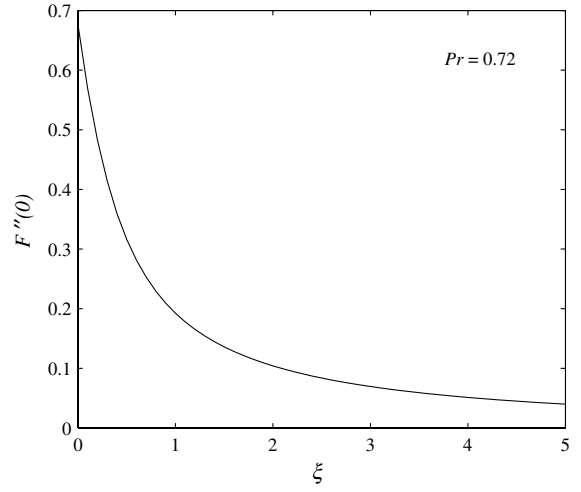


**Fig. 6 Skin friction as a function of nonequilibrium.**

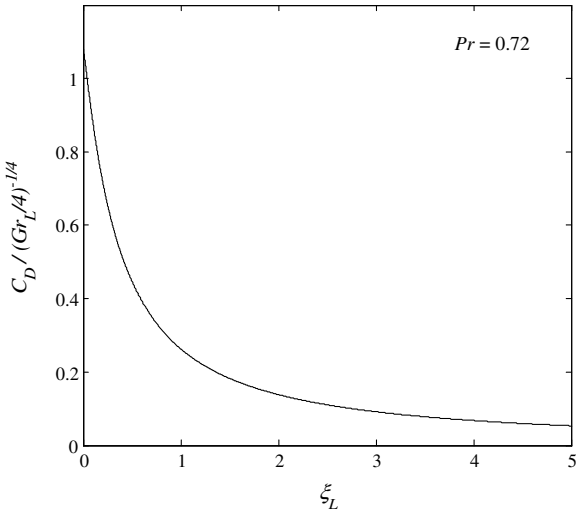


**Fig. 7 Drag coefficient as a function of nonequilibrium ($Pr = 0.72$).**

$$\frac{C_D}{(Gr_L/4)^{-1/4}} = \frac{8}{5}F''(0) \tag{47}$$

Note that $F''(0)$ is equal to 0.6760 at the no-slip condition for $Pr$ of 0.72 [35], and hence the no-slip drag coefficient based on Eq. (47) gives 1.0816. Therefore, the result based on the integration form gives only a 0.1% difference from the classical no-slip value. Note that the small deviation was mainly caused by the curve-fitting process. Thus, the drag coefficient calculated by the integration formula is able to converge well to the no-slip value, provided the curve fitting of $F''(0)$ is of good accuracy.

The boundary-layer thickness is given by

$$\delta = x\eta_{1\%}(Gr_x/4)^{-1/4} \tag{48}$$

The value where $F'$ is at 1% of the maximum value is in the viscous boundary layer; whereas, in the thermal boundary layer, $\eta_{1\%}$ is the position where the dimensionless temperature $\theta$ reaches the value of 0.01 [35]. The expression of boundary-layer thickness can be substituted into the definition of $\xi$ to obtain

$$\xi = Kn_\delta \eta_{1\%} \tag{49}$$

This indicates that the effect of slip is a function of boundary-layer thickness. Figure 8 shows the value of $\eta_{1\%}$ as a function of nonequilibrium $\xi$. The result suggests that the variation in thickness of the momentum boundary layer will generally increase with the nonequilibrium, but a local decrease has been predicted in the slightly rarefied condition for $\xi$ less than 0.2. The behavior of the viscous boundary-layer thickness suggests that the transition to turbulence in gaseous flows could be delayed at slightly rarefied conditions, that is, $\xi < 0.2$, but could also be accelerated as the flow becomes more rarefied. The thermal boundary-layer thickness initially decreases with the increasing nonequilibrium for $\xi$ less than 1.0 and then remains roughly constant. The variation is about 11% for viscous and 6% for thermal boundary-layer thickness between the no-slip condition and $\xi$ at 5.0. Note also that, at the no-slip condition, the viscous and thermal boundary-layer thickness $\eta_{1\%}$ gives 5.497 and 4.401, respectively, which agrees with the no-slip boundary-layer thickness value of 5.5 and 4.42 reported in [35].

Figure 9 shows the wall temperature as a function of nonequilibrium for varying Prandtl 0.6, 0.7, 0.8, 0.9, and 1.0. These Prandtl numbers can represent typical values for air and other gasses around room temperature. The amount of temperature jump will increase substantially with the increased nonequilibrium, that is, the percentage drop is more than 75% between the no-slip condition and $\xi$ at 5.0 for $Pr$ of 0.7. One may also expect that, as $\xi$ approaches a sufficient large value, the temperature jump as a result will become infinitely large, giving a uniform temperature distribution within the boundary layer. The result also suggests that, for a given value of $\xi$, the amount of temperature jump will increase with the decreasing $Pr$.

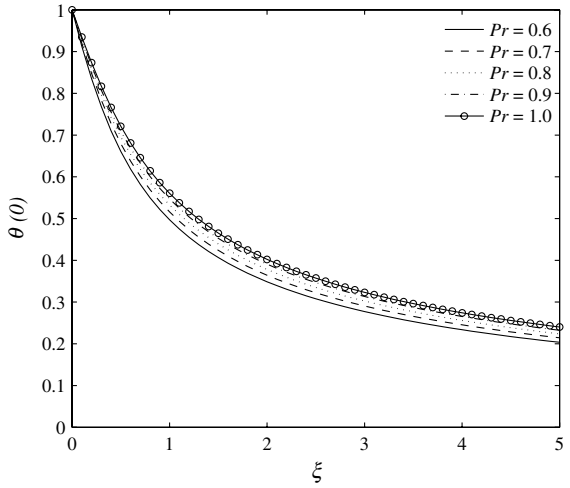


**Fig. 9 Dimensionless wall temperature.**

The dimensionless local heat transfer is proportional to the magnitude of the local wall temperature gradient, given by $Nu_x/(Gr_x/4)^{1/4} = -\theta'(\xi, 0)$. The local heat transfer at the plate (i.e., the wall temperature gradient) as a function of Prandtl number and nonequilibrium is plotted in Fig. 10. The results show that the heat transfer tends to decrease as the flow becomes more rarefied, causing an approximately 80% decrease as $\xi$ varies from 0 to 5.0. This behavior is due to a combinational effect of the simultaneous velocity slip and thermal jump conditions imposed at the wall. Although it is expected that the enhanced velocity due to slip near the plate will increase the local heat transfer (as will be seen shortly in liquid flow), the existing wall temperature jump plays a counteractive role in decreasing the heat transfer. The attenuation in heat transfer caused by the thermal jump condition outweighs the increased amount caused by the slip velocity, thereby resulting in a decreasing local heat transfer with rarefaction. It is also seen that the local heat transfer will be enhanced with increasing Prandtl number for an identical rarefaction condition. Note that the current result of local heat transfer is contradictory to that reported in [30], where an increase was observed with an increasing $Kn$. This discrepancy is due to the fact that only the velocity slip was considered in [30]. The velocity slip, by itself, will result in an increased heat transfer due to the enhanced velocity field near the plate. However, the variation of local heat transfer with Prandtl number agrees with the trend shown in [30].

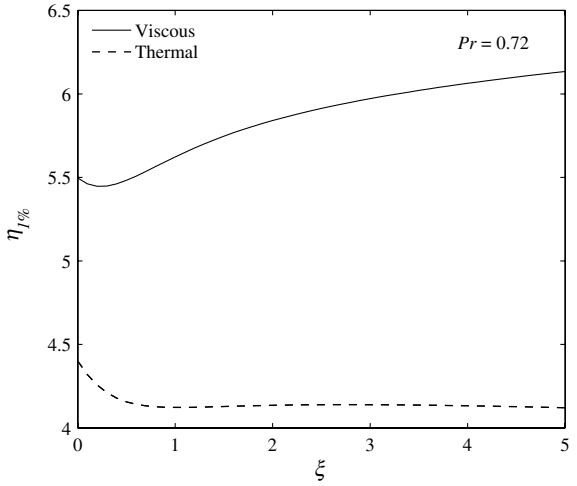


**Fig. 8 Boundary-layer thickness as a function of nonequilibrium ($Pr = 0.72$).**

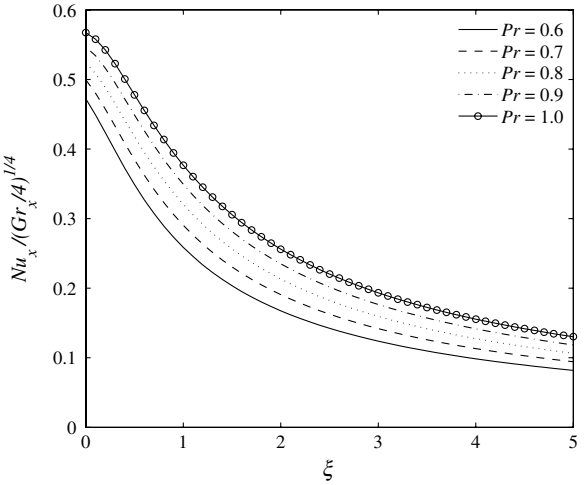


**Fig. 10 Wall temperature gradient.**

The average heat transfer coefficient may be defined as

$$\bar{h} = \frac{1}{L}\int_0^L h\,\mathrm{d}x = \frac{k}{L}\left[\frac{g\beta(T_s - T_\infty)}{4\nu^2}\right]^{1/4}\int_0^L -\theta'(\xi,0)x^{-1/4}\,\mathrm{d}x \tag{50}$$

and thus the average Nusselt number over the entire plate is given by

$$\overline{Nu}_L = \left[\frac{g\beta(T_s - T_\infty)}{4\nu^2}\right]^{1/4}\int_0^L -\theta'(\xi,0)x^{-1/4}\,\mathrm{d}x \tag{51}$$

In terms of the definition of $\xi$, given in Eq. (14), the expression for the average Nusselt number can be derived as an integral formula:

$$\frac{\overline{Nu}_L}{(Gr_L/4)^{1/4}} = 4\xi_L^3\int_{\xi_L}^{\infty} -\theta'(\xi,0)\xi^{-4}\,\mathrm{d}\xi \tag{52}$$

Note $\theta'(\xi,0)$ contained in the integral is a function of both $\xi$ and $Pr$. For a given Prandtl number, the temperature gradient, however, is a function of $\xi$ only. The relation between $-\theta'(\xi,0)$ and $\xi$ can therefore be obtained by fitting to the curve shown in Fig. 10. Take $Pr$ of 0.7, for example, the wall temperature gradient can be fitted as a function of the nonsimilarity variable through

$$\frac{Nu_x}{(Gr_x/4)^{1/4}} = \frac{0.9047}{1.781 + 1.321\xi^{1.133}} \tag{53}$$

The preceding correlation gives a coefficient of determination of 0.9994. The average Nusselt number was then obtained by substituting the preceding expression into Eq. (52) for numerical integration, and the result is plotted in Fig. 11. It is evident that the heat transfer will decrease significantly with the increasingly rarefied flow, giving more than an 85% drop as $\xi$ varies from the no-slip condition to highly rarefied flow at $\xi$ equal to 5.0.

It is also seen in Fig. 11 that the average Nusselt number is approximately 0.675 as $\xi$ approaches zero. Note that, if at no-slip condition $\theta'(\xi,0)$ becomes independent of $\xi$, so Eq. (52) can be simply integrated to obtain

$$\frac{\overline{Nu}_L}{(Gr_L/4)^{1/4}} = -\frac{4}{3}\theta'(\xi,0) \tag{54}$$

The preceding equation coincides with the average Nusselt number correlation derived at the no-slip condition [34]. According to the wall temperature gradient value reported in [35], the average Nusselt number at the no-slip condition for $Pr$ of 0.7 gives 0.666. The difference is less than 1.4% between the result based on the integration and the classical no-slip value. Note that the small deviation stems mainly from the curve-fitting process of $\theta'(\xi,0)$, but not from the integration itself. The obtained average Nusselt number as a function of nonequilibrium conditions is considered to be able to converge to the no-slip solution as $\xi$ approaches zero. The foregoing procedures can be repeated to determine the average Nusselt number for an arbitrary Prandtl number, provided the curve-fitting process is of acceptable accuracy.

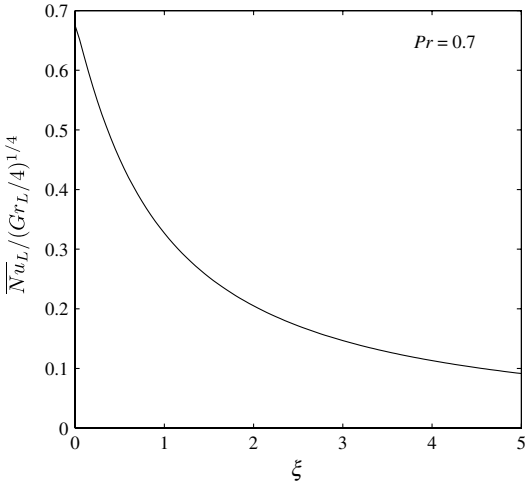


**Fig. 11 Average Nusselt number as a function of nonequilibrium ($Pr = 0.7$).**

### B. Effect of Slip in Liquid Flow

The foregoing section has discussed the effect of simultaneous velocity slip and temperature jump at the wall boundary in gaseous flows. In this subsection, the discussion is extended to examine the effects of slip upon natural convection in liquids. As far as the microscale heat transfer is concerned for liquids, it is usually assumed that there is no wall temperature jump accompanying with the momentum slip [31]. Thus, the temperature at the wall is replaced with the no-thermal-jump condition

$$\theta(0) = 0 \tag{55}$$

Other boundary conditions remain unaltered. Numerical solutions have been first obtained for $Pr$ of 7.0 with varying rarefied conditions. This Prandtl number can represent natural convective slip flow in water at room temperatures.

The velocity profile for Prandtl number of 0.72 with $\xi$ varying from 0 to 5.0 is shown in Fig. 12. It is seen that the velocity profiles for highly rarefied flows, that is, $\xi$ of 5.0, are significantly altered from the no-slip case. The peak velocity is seen to increase as the flow becomes more rarefied, causing more than a 100% increase as $\xi$ varies from no-slip to highly rarefied flow at $\xi$ of 5.0. In addition, the distance where the peak velocity is obtained is found to shift toward the plate with increasing $\xi$. This behavior is a result of the increasing slip velocity at the wall.

The temperature distribution as a function of nonequilibrium for $Pr$ of 7.0 is shown in Fig. 13. Although no temperature jump exists in this case, the dimensionless temperature at a given location $\eta$ will still decrease as the flow becomes more rarefied. For instance, for slightly rarefied flow of $\xi$ equal to 1.0, the temperature at the position $\eta$ of 1.0 is 60% lower than the no-slip value. This is because the increased velocity field near the plate due to the slip condition results in an enhanced heat transfer rate from the plate to the surroundings, thereby rapidly reducing the temperature of fluid near the wall.

Figure 14 shows the 2-D contour plot of the stream function for $Pr = 7.0$ as a function of position and nonequilibrium. At any given position $\eta$ in the boundary layer, the value of stream function $F$ will increase as the flow becomes more rarefied. Note that the difference between stream functions indicates the volume flow rate per unit depth. As the flow proceeds along the plate, the value of $\xi$ decreases, and the slip velocity near the plate also decreases, leading to a decrease in flow rate along the plate.

Figure 15 shows the slip velocity at the plate for $Pr$ of 7.0. The slip velocity at the wall increases monotonically with the increased

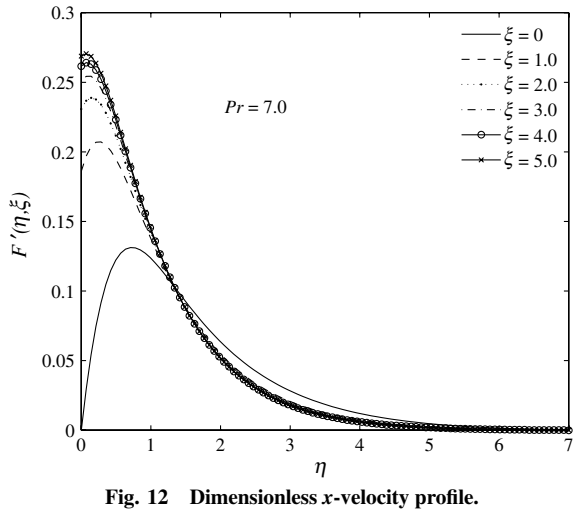


**Fig. 12 Dimensionless $x$-velocity profile.**

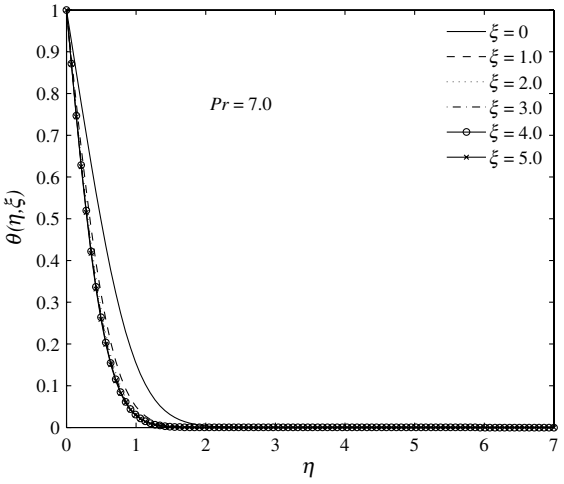


**Fig. 13 Dimensionless temperature profile.**

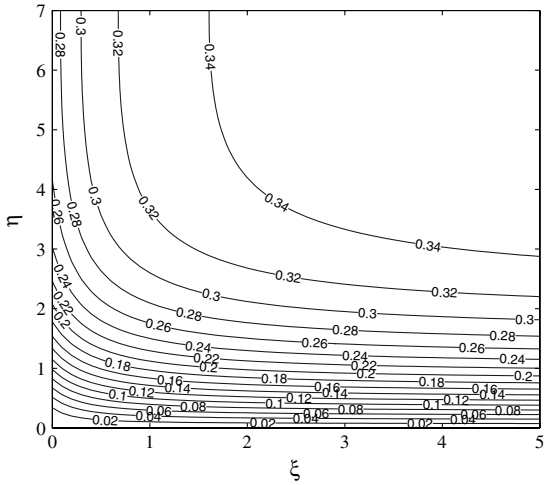


**Fig. 14 Stream function as a function of $\eta$ and $\xi$ ($Pr = 7.0$).**

rarefaction. This is a direct result of the imposed momentum slip boundary condition at the wall. The slip velocity reaches approximately 0.269 when $\xi$ is equal to 5.0.

Figure 16 shows the dimensionless wall shear stress for $Pr$ of 7.0. The result shows that $F''(0)$ will decrease as the flow becomes more rarefied, leading to more than an 85% drop as $\xi$ varies from 0 to 5.0. At $\xi$ equal to zero, the value of $F''(0)$ is 0.4507, which also agrees well with the no-slip value recorded in [35].

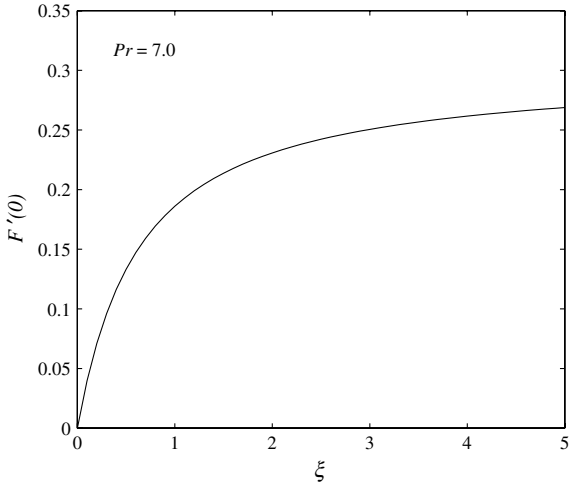


**Fig. 15 Slip velocity as a function of nonequilibrium.**

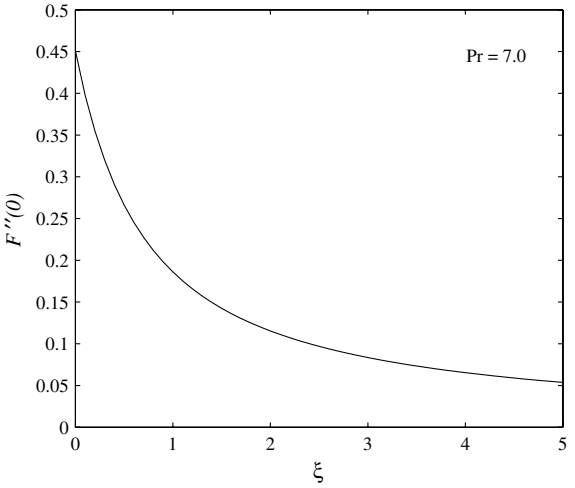


**Fig. 16 Wall shear stress as a function of nonequilibrium.**

The thickness of the viscous and thermal boundary layers was calculated based on the definition of $\eta_{1\%}$ described in the previous subsection. Figure 17 shows the value of $\eta_{1\%}$ as a function of $\xi$ for $Pr$ of 7.0. The result suggests that the thickness of both the viscous and thermal boundary layer will decrease with the increasingly rarefied flow. The percentage variation in thickness is approximately 22% for the viscous boundary layer and 32% for the thermal boundary layer as the flow deviates from the no-slip condition. The result suggests the transition to turbulence could be delayed for natural convection in liquids, that is, water flow.

Figure 18 shows the local heat transfer on the plate [i.e., the wall temperature gradient $-\theta'(0)$] as a function of nonequilibrium for $Pr$ of 2.0, 3.0, 5.0, 7.0, and 10.0. Note the local heat transfer value is equal to $-\theta'(0)$. The result shows that the local heat transfer at the plate will increase with the increased rarefaction condition for liquids. In addition, it is seen that the amount of increase in $Nu_x/(Gr_x/4)^{1/4}$ will increase as the Prandtl number becomes larger, that is, approximately 50% for $Pr$ of 2.0 and 82% for $Pr$ of 10.

The average Nusselt number over the entire plate can be computed according to Eq. (52). Before the integration can be performed, $-\theta'(0)$ needs to be expressed as a function of $\xi$. The flow with $Pr$ of 7.0 is used as an illustration for which the average Nusselt number is to be obtained. By curve fitting, $-\theta'(0)$ for a $Pr$ of 7.0 can be expressed by an interpolation formula of the form

$$\frac{Nu_x}{(Gr_x/4)^{1/4}} = 1.925 - \frac{8.796}{10.09 + 16.73\xi^{1.098}} \tag{56}$$

The coefficient of determination of the preceding correlation is 0.9999901. Substitute Eq. (56) into Eq. (52) and integrate to yield the

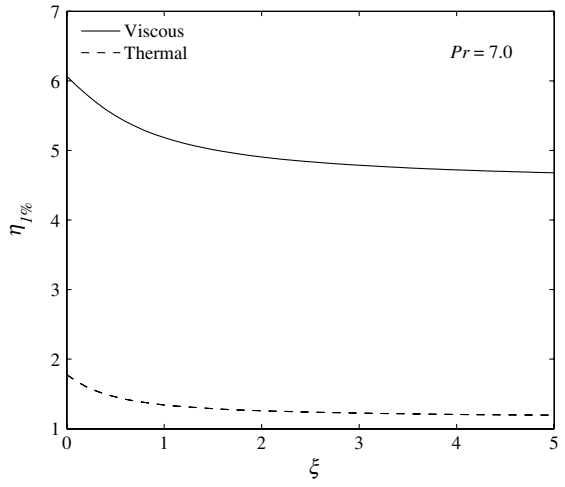


**Fig. 17 Viscous and thermal boundary-layer thickness.**

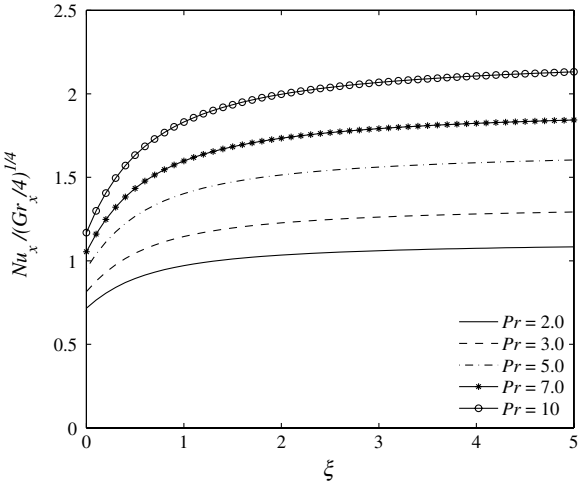


**Fig. 18 Wall temperature gradient.**

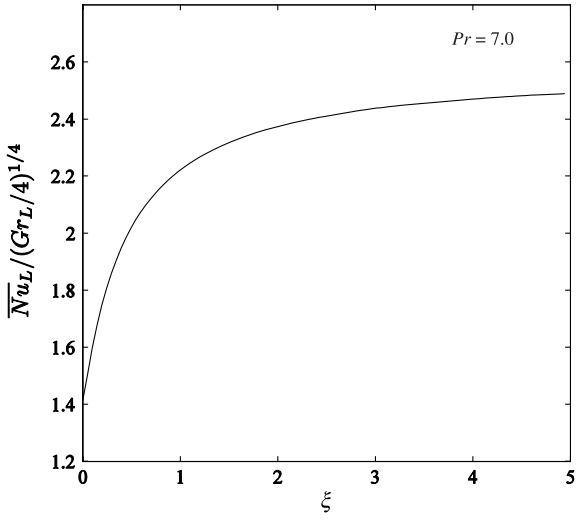


**Fig. 19 Average Nusselt number for liquid flow.**

correlation of $\overline{Nu}_L/(Gr_L/4)^{1/4}$ as a function of nonequilibrium, plotted in Fig. 19. When the result is compared with the no-slip value, it is seen that the average heat transfer over the entire plate will increase greatly as flow becomes more rarefied. The percentage of increase in average heat transfer is approximately 75% as $\xi$ reaches 5.0 for flow with $Pr$ of 7.0. At $\xi$ equal to zero, the value of $\overline{Nu}_L/(Gr_L/4)^{1/4}$ is 1.405. This result can be compared with the no-slip value for the Nusselt number obtained by Eq. (54), which gives about 1.4069, hence, the result gives only a 0.14% difference, so that it agrees well with the classical no-slip value of average heat transfer.

It is also interesting to note that the heat transfer behavior in rarefied liquid flow, shown in Fig. 19, is different than that in gaseous flows, see Fig. 11. In liquids, due to the imposed velocity slip condition at the wall, the flow velocity will be enhanced near the wall, as seen in Fig. 12. Consequently, heat transfer from the plate will be augmented due to the increased velocity field as the flow becomes gradually more rarefied. Nevertheless, in gaseous flows, the presence of the thermal jump condition at the wall will significantly reduce the heat transfer from the plate. As a result, the presence of a thermal jump in gaseous flows offsets the increased heat transfer gained by velocity slip, leading to a decreased heat transfer in gaseous slip flows.

## IV. Conclusions

The boundary-layer equations for natural convective rarefied flow over a vertical flat plate have been solved with first-order slip boundary conditions using local-nonsimilarity transformations. Natural convection boundary-layer velocity and temperature distributions do not admit self-similar solutions for slightly rarefied conditions. The nonequilibrium conditions existing at the wall result in an enhanced velocity field in the vicinity of the plate due to a velocity discontinuity. The peak slip velocity for the gaseous flows examined here was found to exist for moderately rarefied conditions, that is, the maximum wall slip velocity reached 0.2093 at $\xi$ equal to 2.5 for $Pr$ of 0.72. In liquids, the wall slip velocity was found to increase monotonically with an increasing degree of rarefaction. In addition, the slip condition leads to a more rapid decrease in wall shear stress compared with the no-slip condition. For instance, a 95% decrease in gas flow ($Pr = 0.72$) and 85% in liquid ($Pr = 7.0$) was observed as $\xi$ varied from 0 to 5.0.

The heat transfer in the boundary layer was also affected by the presence of interfacial nonequilibrium boundary conditions. In liquid slip flows, the heat transfer was enhanced as a result of the increased velocity near the plate that resulted from the momentum slip at the interface. In gaseous flows, however, the heat transfer decreased as the environment became more rarefied. This behavior was due to the fact that the temperature jump condition reduced the heat transfer more than that enhanced by the wall slip velocity.

Integral formulas for the drag coefficient, Eq. (45), and the average Nusselt number, Eq. (52), as a function of the nonequilibrium parameter were developed. These relations will be useful for future analysis of natural convective flow in microdevices and in slightly rarefied environments, that is, those associated with near-space applications.

## Acknowledgments

This work has been supported by the University of Alabama's College of Engineering through the Alton Scott Research Working Group Program and by a University Graduate Council Fellowship. The authors would also like to acknowledge the Alabama Space Grant Consortium, whose initial support for the undergraduate balloonsat program at the University of Alabama motivated this work.

## References

[1] Ostrach, S., "An Analysis of Laminar Free-Convection Flow and Heat Transfer About a Flat Plate Parallel to the Direction of the Generating Body Force," NACA TR-1111, 1953.

[2] Zubair, S. M., and Kadaba, P. V., "Similarity Transformations for Boundary Layer Equations in Unsteady Mixed Convection," *International Communications in Heat and Mass Transfer*, Vol. 17, No. 2, 1990, pp. 215–226. doi:10.1016/0735-1933(90)90055-O

[3] Sparrow, E. M., Eichhorn, R., and Gregg, J. L., "Combined Forced and Free Convection in a Boundary Layer Flow," *Physics of Fluids*, Vol. 2, No. 3, 1959, pp. 319–328. doi:10.1063/1.1705928

[4] Sparrow, E. M., Quack, H., and Boerner, C. J., "Local Nonsimilarity Boundary-Layer Solutions," *AIAA Journal*, Vol. 8, No. 11, 1970, pp. 1936–1942. doi:10.2514/3.6029

[5] Sparrow, E. M., and Yu, H. S., "Local Non-Similarity Thermal Boundary-Layer Solutions," *Journal of Heat Transfer*, Vol. 93, Nov. 1971, pp. 328–334.

[6] Hieber, C. A., "Natural Convection Around a Semi-Infinite Vertical Plate: Higher-Order Effects," *International Journal of Heat and Mass Transfer*, Vol. 17, No. 7, 1974, pp. 785–791. doi:10.1016/0017-9310(74)90172-0

[7] Riley, D. S., and Drake, D. G., "Higher Approximations to the Free Convection Flow from a Heated Vertical Plate," *Applied Scientific Research*, Vol. 30, No. 3, 1975, pp. 193–207. doi:10.1007/BF00705746

[8] Mahajan, R. L., and Gebhart, B., "Higher Order Approximations to the Natural Convection Flow over a Uniform Flux Vertical Surface," *International Journal of Heat and Mass Transfer*, Vol. 21, No. 5, 1978, pp. 549–556. doi:10.1016/0017-9310(78)90051-0

[9] Martynenko, O. G., Berezovsky, A. A., and Sokovishin, Y. A., "Laminar Free Convective from a Vertical Plate," *International Journal*

*of Heat and Mass Transfer*, Vol. 27, No. 6, 1984, pp. 869–881. doi:10.1016/0017-9310(84)90008-5

[10] Giordano, N., and Cheng, J. T., "Microfluid Mechanics: Progress and Opportunities," *Journal of Physics: Condensed Matter*, Vol. 13, No. 15, 2001, pp. R271–R295. doi:10.1088/0953-8984/13/15/201

[11] Cao, K., and Baker, J., "Application of Transient Network Models for Near Space Thermal Management," AIAA Paper 2008-1192, 2008.

[12] Karniadakis, G., Beskok, A., and Aluru, N., *Microflows and Nanoflows*, Springer, New York, 2005, Chap. 1.

[13] Gad-el-Hak, M., "Fluid Mechanics of Microdevices: The Freeman Scholar Lecture," *Journal of Fluids Engineering*, Vol. 121, No. 1, 1999, pp. 5–33. doi:10.1115/1.2822013

[14] Maxwell, J. C., "On Stresses in Rarefied Gases Arising from Inequalities of Temperature," *Philosophical Transactions of the Royal Society of London*, Pt. 1, Vol. 170, 1879, pp. 231–256. doi:10.1098/rstl.1879.0067

[15] McNenly, M. J., Gallis, M. A., and Boyd, I. D., "Slip Model Performance for Micro-Scale Gas Flows," AIAA Paper 2003-4050, June 2003.

[16] Bahukudumbi, P., Park, J. H., and Beskok, A., "A Unified Engineering Model for Steady and Quasi-Steady Shear-Driven Gas Microflows," *Microscale Thermophysical Engineering*, Vol. 7, No. 4, 2003, pp. 291–315. doi:10.1080/10893950390243581

[17] Beskok, A., "A Model for Flows in Channels, Pipes, and Ducts at Micro and Nano Scales," *Microscale Thermophysical Engineering*, Vol. 3, No. 1, 1999, pp. 43–77. doi:10.1080/108939599199864

[18] Pan, L. S., Liu, G. R., and Lam, K. Y., "Determination of Slip Coefficient for Rarefied Gas Flows Using Direct Simulation Monte Carlo," *Journal of Micromechanics and Microengineering*, Vol. 9, No. 1, 1999, pp. 89–96. doi:10.1088/0960-1317/9/1/312

[19] Bayazitoglu, Y., and Tunc, G., "An Extension to the First Order Slip Boundary Conditions to Be Used in Early Transition Regime," AIAA Paper 2002-2779, June 2002.

[20] McNenly, M. J., Gallis, M. A., and Boyd, I. D., "Empirical Slip and Viscosity Model Performance for Microscale Gas Flow," *International Journal for Numerical Methods in Fluids*, Vol. 49, No. 11, 2005, pp. 1169–1191. doi:10.1002/fld.1012

[21] White, F. M., *Viscous Fluid Flow*, 3rd ed., McGraw–Hill, New York, 2006, Chap. 1.

[22] Tretheway, D. C., and Meinhart, C. D., "Apparent Fluid Slip at Hydrophobic Microchannel Walls," *Physics of Fluids*, Vol. 14, No. 3, 2002, pp. L9–L12. doi:10.1063/1.1432696

[23] Ho, C. M., and Tai, Y. C., "Micro-Electro-Mechanical-Systems (MEMS) and Fluid Flows," *Annual Review of Fluid Mechanics*, Vol. 30, Jan. 1998, pp. 579–612.

[24] Mala, M. G., and Li, D., "Flow Characteristics of Water in Microtubes," *International Journal of Heat and Fluid Flow*, Vol. 20, No. 2, 1999, pp. 142–148. doi:10.1016/S0142-727X(98)10043-7

[25] Obot, N. T., "Toward a Better Understanding of Friction and Heat/Mass Transfer in Microchannels: A Literature Review," *Microscale Thermophysical Engineering*, Vol. 6, No. 3, 2002, pp. 155–173. doi:10.1080/10893950290053295

[26] Koo, J., and Kleinstreuer, C., "Liquid Flow in Microchannels: Experimental Observations and Computational Analyses of Microfluidics Effects," *Journal of Micromechanics and Microengineering*, Vol. 13, No. 5, 2003, pp. 568–579. doi:10.1088/0960-1317/13/5/307

[27] Stone, H. A., Stroock, A. D., and Ajdari, A., "Engineering Flows in Small Devices: Microfluidics Toward a Lab-on-a-Chip," *Annual Review of Fluid Mechanics*, Vol. 36, Jan. 2004, pp. 381–411.

[28] Neto, C., Evans, D. R., Bonaccurso, E., Butt, H.-J., and Craig, V. S. J., "Boundary Slip in Newtonian Liquids: A Review of Experimental Studies," *Reports on Progress in Physics*, Vol. 68, No. 12, 2005, pp. 2859–2897. doi:10.1088/0034-4885/68/12/R05

[29] Oosthuizen, P. H., "The Effect of Surface Slip on the Laminar Free Convective Heat Transfer from an Isothermal Vertical Flat Plate," *Applied Scientific Research*, Vol. 16, No. 1, 1966, pp. 121–130. doi:10.1007/BF00384059

[30] Eldighidy, S. M., and Fathalah, K. A., "Effect of the Slip Boundary Condition on Natural Convection Heat Transfer From an Isothermal Vertical Plate," *Journal of Engineering and Applied Sciences*, Vol. 1, No. 2, 1981, pp. 129–138.

[31] Martin, M. J., and Boyd, I. D., "Momentum and Heat Transfer in a Laminar Boundary Layer with Slip Flow," *Journal of Thermophysics and Heat Transfer*, Vol. 20, No. 4, 2006, pp. 710–719. doi:10.2514/1.22968

[32] Kierzenka, J., and Shampine, L. F., "A BVP Solver Based on Residual Control and the MATLAB PSE," *ACM Transactions on Mathematical Software*, Vol. 27, No. 3, 2001, pp. 299–316. doi:10.1145/502800.502801

[33] Shampine, L. F., Gladwell, I., and Thompson, S., *Solving ODEs with MATLAB*, Cambridge Univ. Press, Cambridge, England, U.K., 2003.

[34] Incropera, F. P., and DeWitt, D. P., *Introduction to Heat Transfer*, 4th ed., Wiley, New York, 2001, Chaps. 7–9.

[35] Gebhart, B., Jaluria, Y., Mahajan, R. L., and Sammakia, B., *Buoyancy-Induced Flows and Transport*, Textbook ed., Hemisphere, New York, 1988, Chap. 3.